arXiv:1609.04942v1 [nucl-th] 16 Sep 2016

Linearly increasing radius of the light fragment during the spontaneous fission of ^{282}Cn

D. N. Poenaru* and R. A. Gherghescu*

Horia Hulubei National Institute of Physics and Nuclear Engineering (IFIN-HH), P.O. Box MG-6, RO-077125 Bucharest-Magurele, Romania and Frankfurt Institute for Advanced Studies, Johann Wolfgang Goethe University, Ruth-Moufang-Str. 1, D-60438 Frankfurt am Main, Germany

(Dated:)

Abstract

In a previous article published in Phys. Rev. C 94 (2016) 014309 we have shown for the first time that the best dynamical trajectory during the deformation toward fission of the superheavy nucleus ^{286}Fl is a linearly increasing radius of the light fragment, R_2. This macroscopic-microscopic result reminds us about the α or cluster preformation at the nuclear surface, assumed already in 1928, and proved microscopically many times. This time we give more detailed arguments for the neighboring nucleus ^{282}Cn. Also similar figures are presented for heavy nuclei ^{240}Pu and ^{252}Cf. The deep minimum of total deformation energy near the surface is shown for the first time as a strong argument for cluster preformation.

PACS numbers: 25.85.Ca, 24.75.+i, 21.10.Tg, 27.90.+b

* poenaru@fias.uni-frankfurt.de

I. INTRODUCTION

The most important decay modes of superheavy nuclei are mainly α decay and spontaneous fission [1–9]. Among the many theoretical papers in this field one should mention [10–14] and [15–22]. For atomic numbers larger than 121 cluster decay [23, 24] may compete as well [25, 26].

In 1928 G. Gamow [27] as well as R.W. Gurney and E.U. Condon [28] gave the first explanation of α decay based on quantum mechanical tunneling of a preformed particle at the nuclear surface. The microscopic theory had been developed by many scientists, e.g. [29–35]. It was also extended to explain cluster decays [35–37]. Simple relationships are also very useful [11, 38].

In our paper mentioned in the abstract [39] we reported results obtained within macroscopic-microscopic method [40] using cranking inertia [41, 42] and the best two-center shell model [43] in the plane of two independent variables (R, η), where R is the separation distance of the fragments and $\eta = (A_1 - A_2)/A$ is the mass asymmetry with A, A_1, A_2 the mass numbers of the parent and nuclear fragments. Phenomenological deformation energy, E_{Y+E}, was given by Yukawa-plus-exponential model [44], and the shell plus pairing corrections, $\delta E = \delta U + \delta P$ are based on the asymmetric two center shell model (ATCSM) [43]. This time we give more detailed arguments for the neighboring nucleus ^{282}Cn. Also similar figures are presented for heavy nuclei ^{240}Pu and ^{252}Cf. The deep minimum of total deformation energy near the surface is shown for the first time as a strong argument for cluster preformation.

II. MODEL

An outline of the model was presented previously [39]. We repeat few lines in this section. The parent ^{A}Z is split in two fragments: the light, $^{A_2}Z_2$, and the heavy one, $^{A_1}Z_1$ with conservation of hadron numbers $A = A_1 + A_2$ and $Z = Z_1 + Z_2$. The corresponding radii are given by $R_0 = r_0 A^{1/3}$, $R_{2f} = r_0 A_2^{1/3}$, and $R_{1f} = r_0 A_1^{1/3}$. The separation distance of the fragments is initially $R_i = R_0$ and at the touching point $R_t = R_{1f} + R_{2f}$ with $r_0 = 1.16$ fm.

The geometry for linearly increasing R_2 from 0 to $R_{2f} = R_e$ is defined by:

$$R_2 = R_{2f} \frac{R - R_i}{R_t - R_i} \tag{1}$$

According to the macroscopic-microscopic method the total deformation energy contains

the Yukawa-plus-exponential (Y+EM) and the shell plus pairing corrections

$$E_{def} = E_{Y+E} + \delta E \tag{2}$$

In units of $\hbar\omega_0^0 = 41A^{-1/3}$ the shell corrections are calculated with the Strutinsky procedure as a sum of protons and neutrons contributions

$$\delta u = \delta u_p + \delta u_n \tag{3}$$

By solving the BCS [45] system of two equations with two unknowns, we find the Fermi energy, λ, and the pairing gap Δ. The total pairing corrections are given by

$$\delta p = \delta p_p + \delta p_n \tag{4}$$

and finally the total shell plus pairing corrections in MeV

$$\delta E = \delta U + \delta P \tag{5}$$

The inertia tensor [42] is given by

$$B_{ij} = 2\hbar^2 \sum_{\nu\mu} \frac{\langle\nu|\partial H/\partial\beta_i|\mu\rangle\langle\mu|\partial H/\partial\beta_j|\nu\rangle}{(E_\nu + E_\mu)^3}(u_\nu v_\mu + u_\mu v_\nu)^2 \tag{6}$$

where H is the single-particle Hamiltonian allowing to determine the energy levels and the wave functions $|\nu\rangle$, u_ν^2, v_ν^2 are the BCS occupation probabilities, E_ν is the quasiparticle energy, and β_i, β_j are the independent shape coordinates. For spherical fragments with R, R_2 deformation parameters the cranking inertia symmetrical tensor will have three components, hence the scalar

$$B(R) = B_{R_2R_2}\left(\frac{dR_2}{dR}\right)^2 + 2B_{R_2R}\frac{dR_2}{dR} + B_{RR} = B_{22} + B_{21} + B_{11} \tag{7}$$

When we find the least action trajectory in the plane (R, R_2) we need to calculate the three components B_{22}, B_{21}, B_{11} in every point of a grid of 66×24 (for graphics) or 412×24 (for the real calculation) for 66 or 412 values of $(R-R_i)/(R_t-R_i)$ and 24 values of $\eta = (A_1-A_2)/A$ or R_{2f}.

III. RESULTS

Potential energy surfaces (PES) for spontaneous fission of ^{282}Cn are shown in figures 1 and 2 for constant radius, R_2, of the light fragment and linearly increasing one, respectively.

The corresponding contour plots are given in figures 3 and 4, where the first and second minima of deformation energy at every value of mass asymmetry are plotted with dashed and dotted white lines. More details are given in the two tables II and I. Also, the position and value of maximum Y+EM model deformation energy versus mass asymmetry, η, for fission of ^{282}Cn with linearly increasing R_2 (top) and constant R_2 (bottom) are shown in figure 10.

In figure 5 we compare the deformation energies with respect to spherical shapes for symmetrical fission of ^{282}Cn with R_2 constant and linearly increasing R_2 (Lin). One can see a relatively law macroscopic energy E_{Y+ELin} on which the shell and pairing corrections, $\delta ELin$ deegs a rather deep minimum not far from the nuclear surface. A completely different "classical" two-humped barrier, E_{def}, may be seen for $R_2 =$ constant. While the first minima in figure 4 and table I, are all lying at $x = 0$, this is true only for 10 mass asymetries out of 23 in figure 3 and the table II.

We compare in figure 6 the absolute values of shell and pairing correction energies for symmetrical fission of ^{282}Cn with R_2 constant (dashed line) and linearly increasing R_2 (solid line). As expected, the gap for protons, Δ_p, and neutrons, Δ_n, solutions of the BCS system of two equations, in figure 7 are also following similar variations, while the Fermi energies, λ_p and λ_n have only a shallow minima in the surface region. Deep minima around $(R - R_i)/(R_t - R_i) = 0.82$ are clearly seen in both figures. Similar results are also obtained for heavy nuclei like ^{240}Pu, figure 8 and ^{252}Cf (see figure 9). See also figures 1-3 of the e-print [47]. At the touching point, $R = R_t$, both kinds of variations of $R_2 = R_2(R)$ are ariving at the same state, hence the shell effects are identical there, as may be seen in figures 6, 8 and 9.

The decimal logarithm of the dimensionles B_{RR}/m component of nuclear inertia tensor for symmetrical fission of ^{282}Cn with linearly increasing R_2 isplotted in figure 11. At the touching point and beyond, $R \geq R_t$, one should get the reduced mass: $B(R \geq R_t) = mA_1A_2/A$. The proton contribution are more important than the neutron one. This figure is completely different from the figure 5 of the Ref.[46] where the components B_{RR}/m for almost symmetrical fission (with the light fragment ^{130}Pd, ^{134}Cd and ^{132}Sn) of ^{282}Cn are shown for $R_2 =$ constant. Values larger than 10^5 are seen in figure 11, compared to smaller than 1.6×10^3 for $R_2 =$ constant.

If we use in graphics $x = (R - R_i)/(R_t - R_i)$ instead of R then for ^{286}Fl the interval of

variation will be $x = (0, 1)$. For the initial parent nucleus one may have either $x = 0$ or/and $\eta = 1$. This is the reason why the dashed line ends up at the value of $\eta = 0.956$. In present calculations we have used 66 values of x from 0 to 1.3 and 24 values of η from 0 to 1.

For minimization of action we need not only B_{RR} but also the values of $B_{R_2R_2}, B_{R_2R}$ in every point of a grid of 66×24 for 66 values of $(R - R_i)/(R_t - R_i)$ and 24 values of $\eta = (A_1 - A_2)/A$ or R_{2f}. We expect a dynamical path very different from the statical one shown in Fig. 4 with a white dashed line. The optimum value of the parameter zero-point vibration energy, E_v, used to reproduce the experimental value of ^{282}Cn spontaneous fission half-life, $\log_{10} T_f^{exp}(s) = -3.086$.

In conclusion, with our method of calculating the spontaneous fission half-life including macroscopic-microscopic method for deformation energy based on asymmetric two-center shell model, and the cranking inertia for the dynamical part, we may find a sequence of several trajectories one of which gives the least action. Assuming spherical shapes, we found that the shape parametrization with linearly increasing R_2 is more suitable to describe the fission process of SHs in comparison with that of exponentially or linearly decreasing law. It is in agreement with the microscopic finding concerning the preformation of a cluster at the surface, which then penetrates by quantum tunneling the potential barrier.

ACKNOWLEDGMENTS

This work was supported within the IDEI Programme under Contracts No. 43/05.10.2011 and 42/05.10.2011 with UEFISCDI, and NUCLEU Programme PN16420101/2016 Bucharest.

[1] J. Khuyagbaatar *et al.*, Phys. Rev. Lett. **112**, 172501 (2014).

[2] J. H. Hamilton, S. Hofmann, and Y. Oganessian, Ann. Rev. Nucl. Part. Sci. **63**, 383 (2013).

[3] Y. T. Oganessian, Radiochimica Acta **99**, 429 (2011).

[4] S. Hofmann, Radiochim. Acta **99**, 405 (2011).

[5] C. E. Duellmann *et al.*, Phys. Rev. Lett. **104**, 252701 (2010).

[6] K. Morita *et al.*, J. Phys. Soc. Jpn. **76**, 045001 (2007).

[7] Y. T. Oganessian, J. Phys. G: Nucl. Part. Phys. **34**, R165 (2007).

[8] S. Hofmann and G. Münzenberg, Review of Modern Physics **72**, 733 (2000).

[9] G. Audi *et al.*, Chinese Physics, C **36**, 11571286 (2012).

[10] A. Sobiczewski, Radiochimica Acta **99**, 395 (2011).

[11] Y. Wang, S. Wang, Z. Hou, and J. Gu, Phys. Rev. C **92**, 064301 (2015).

[12] A. Sobiczewski, J. Phys. G: Nucl. Part. Phys. **43**, 095106 (2016).

[13] C. Qi, Reviews in Physics **1**, 77 (2016).

[14] Y. Qian, Z. Ren, and D. Ni, Phys. Rev. C **94**, 024315 (2016).

[15] A. Staszczak, A. Baran, and W. Nazarewicz, Physical Review C **87**, 024320 (2013).

[16] M. Warda and L. M. Robledo, Phys. Rev. C **84**, 044608 (2011).

[17] R. Smolanczuk, Phys. Rev. C **56**, 812 (1997).

[18] R. Smolanczuk, J. Skalski, and A. Sobiczewski, Physical Review, C **52**, 1871 (1995).

[19] X. J. Bao *et al.*, Journal of Physics G: Nuclear and Particle Physics **42**, 085101 (2015).

[20] X. Bao, H. Zhang, G. Royer, and J. Li, Nucl. Phys. A **906**, 1 (2013).

[21] K. P. Santhosh, R. K. Biju, and S. Sahadevan, Nuclear Physics A **832**, 220 (2010).

[22] C. Xu, Z. Ren, and Y. Guo, Phys. Rev. C **78**, 044329 (2008).

[23] Encyclopaedia Britannica Online, 2011, http://www.britannica.com/EBchecked/topic/465998/.

[24] *Nuclear Decay Modes*, Ed. D. N. Poenaru (Institute of Physics Publishing, Bristol, UK, 1996).

[25] D. N. Poenaru, R. A. Gherghescu, and W. Greiner, Phys. Rev. C **85**, 034615 (2012).

[26] D. N. Poenaru, R. A. Gherghescu, and W. Greiner, Phys. Rev. Lett. **107**, 062503 (2011).

[27] G. Gamow, Zeitschrift für Physik **51**, 204 (1928).

[28] R. W. Gurney and E. U. Condon, Nature **122**, 439 (1928).

[29] R. G. Thomas, Progress of Theoretical Physics **12**, 253 (1954).

[30] A. M. Lane, Reviews of Modern Physics **32**, 519 (1960).

[31] H. J. Mang, Annual Review of Nuclear Science **14**, 1 (1964).

[32] I. Tonozuka and A. Arima, Nuclear Physics, A **323**, 45 (1979).

[33] T. Fliessbach and S. Okabe, Zeitschrift für Physik, A **320**, 289 (1985).

[34] K. Varga, R. G. Lovas, and R. J. Liotta, Physical Review Letters **69**, 37 (1992).

[35] R. Blendowske, T. Fliessbach, and H. Walliser, in *Nuclear Decay Modes*, Ed. D. N. Poenaru (IOP Publishing, Bristol, 1996), Chap. 7, pp. 337–349.

[36] R. G. Lovas *et al.*, Physics Reports **294**, 265 (1998).

[37] D. Delion, *Theory of particle and cluster emission, Lecture Notes in Physics 819* (Springer, Berlin, 2010).

[38] D. N. Poenaru, M. Ivaşcu, and D. Mazilu, Journal de Physique Lettres **41**, L589 (1980).

[39] D. N. Poenaru and R. A. Gherghescu, Phys. Rev. C **94**, 014309 (2016).

[40] V. M. Strutinsky, Nuclear Physics, A **95**, 420 (1967).

[41] D. R. Inglis, Physical Review **96**, 1059 (1954).

[42] M. Brack *et al.*, Review of Modern Physics **44**, 320 (1972).

[43] R. A. Gherghescu, Physical Review **C 67**, 014309/1 (2003).

[44] H. J. Krappe, J. R. Nix, and A. J. Sierk, Physical Review, C **20**, 992 (1979).

[45] J. Bardeen, L. Cooper, and J. Schrieffer, Physical Review, C **108**, 1175 (1957).

[46] D. N. Poenaru and R. A. Gherghescu, J. Phys. G: Nucl. Part. Phys. **41**, 125104 (2014).

[47] D. N. Poenaru and R. A. Gherghescu, E-print arXiv:1609.00847v1 [nucl-th] 2016.

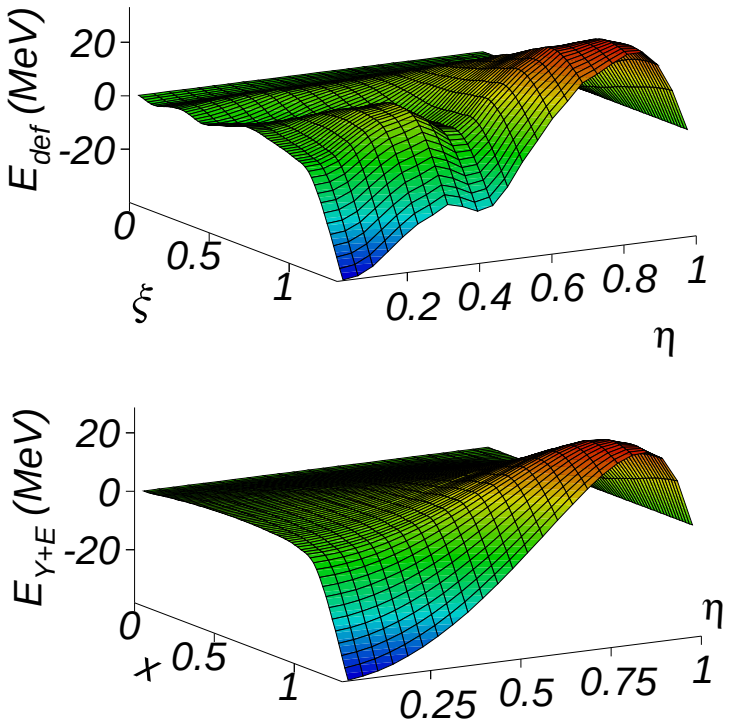


FIG. 1. (Color online) PES of ^{282}Cn vs $(R - R_i)/(R_t - R_i) \geq 0$ and $\eta = (A_1 - A_2)/(A_1 + A_2)$. Y+EM (bottom), and total deformation energy (top). R_2 =constant.

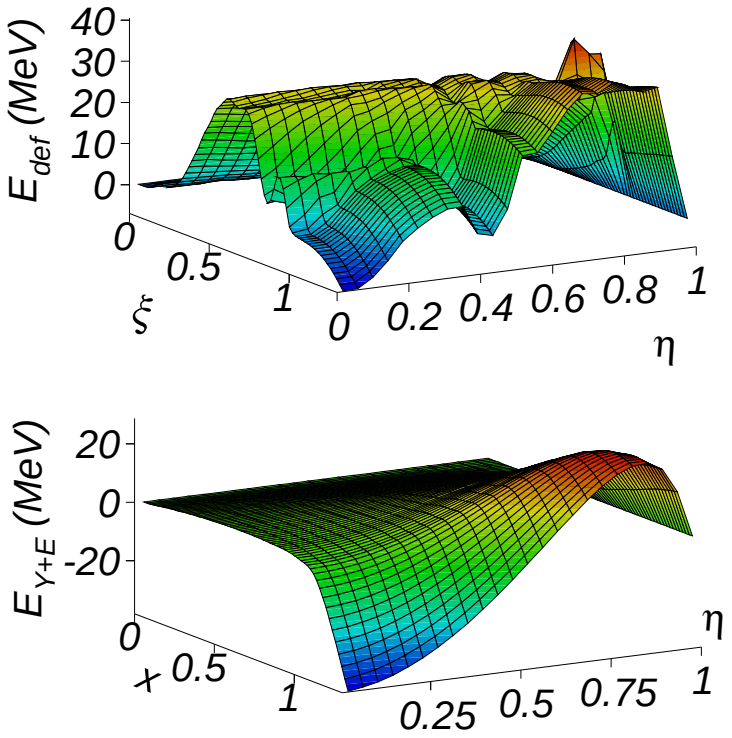


FIG. 2. (Color online) PES of ^{282}Cn vs $(R - R_i)/(R_t - R_i) \geq 0$ and $\eta = (A_1 - A_2)/(A_1 + A_2)$. Y+EM (bottom), and total deformation energy (top). R_2 linearly increasing with R.

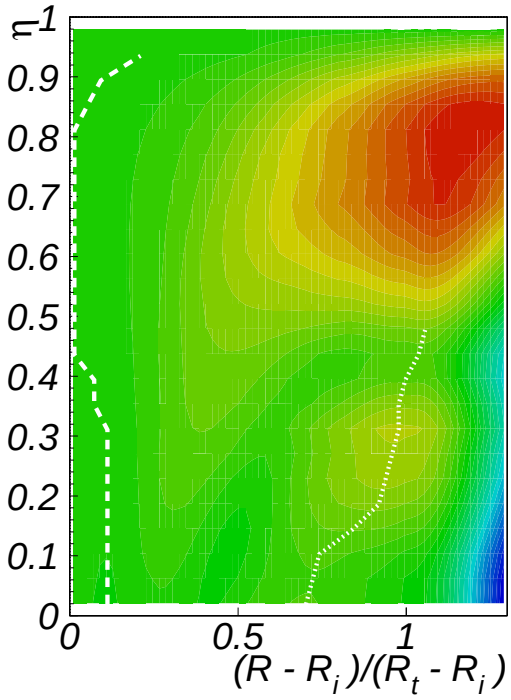


FIG. 3. (Color online) Contour plot of deformation energy of ^{282}Cn shown as a PES in the upper panel of Fig. 1. The first and second minima of deformation energy at every value of mass asymmetry are plotted with dashed and dotted white lines. R_2 =constant.

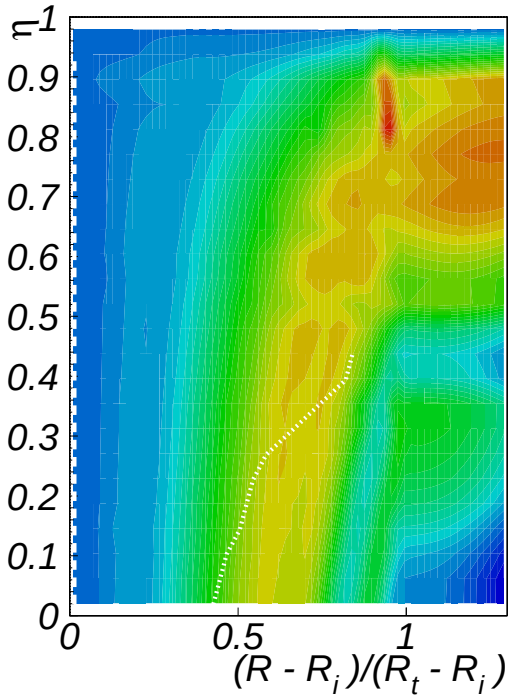


FIG. 4. (Color online) Contour plot of deformation energy of ^{282}Cn shown as a PES in the upper panel of Fig. 2. The first and second minima of deformation energy at every value of mass asymmetry are plotted with dashed and dotted white lines. R_2 linearly increasing with R.

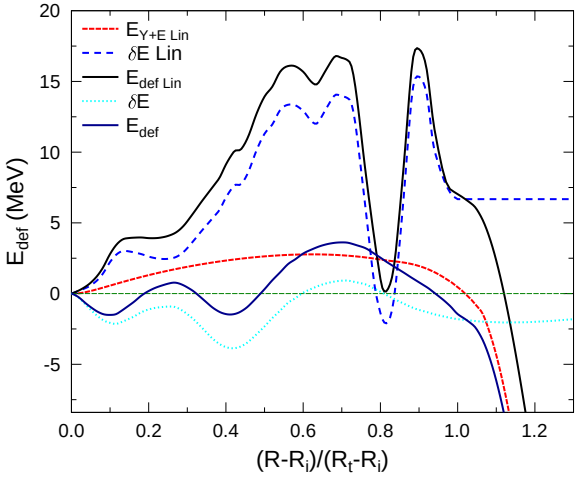


FIG. 5. (Color online) Comparison of deformation energies with respect to spherical shapes for symmetrical fission of ^{282}Cn with R_2 constant and linearly increasing R_2 (Lin).

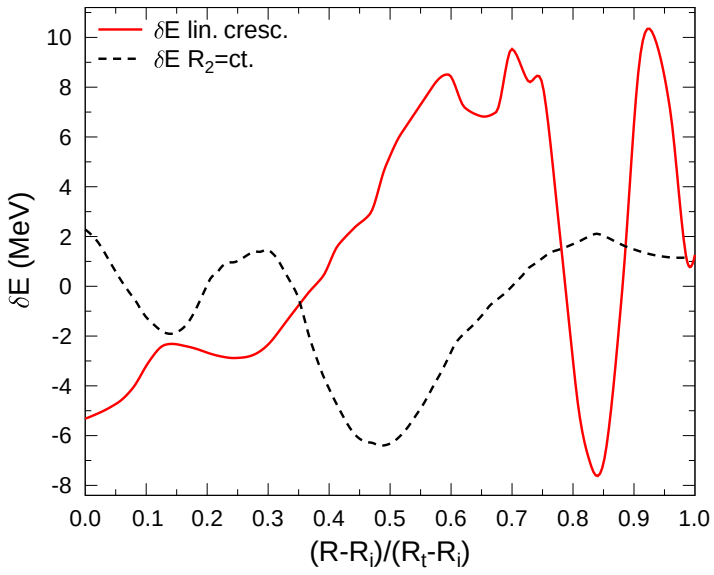


FIG. 6. (Color online) Comparison of absolute values of shell and pairing correction energies for almost symmetrical fission of ^{282}Cn with R_2 constant (dashed line) and linearly increasing R_2 (solid line).

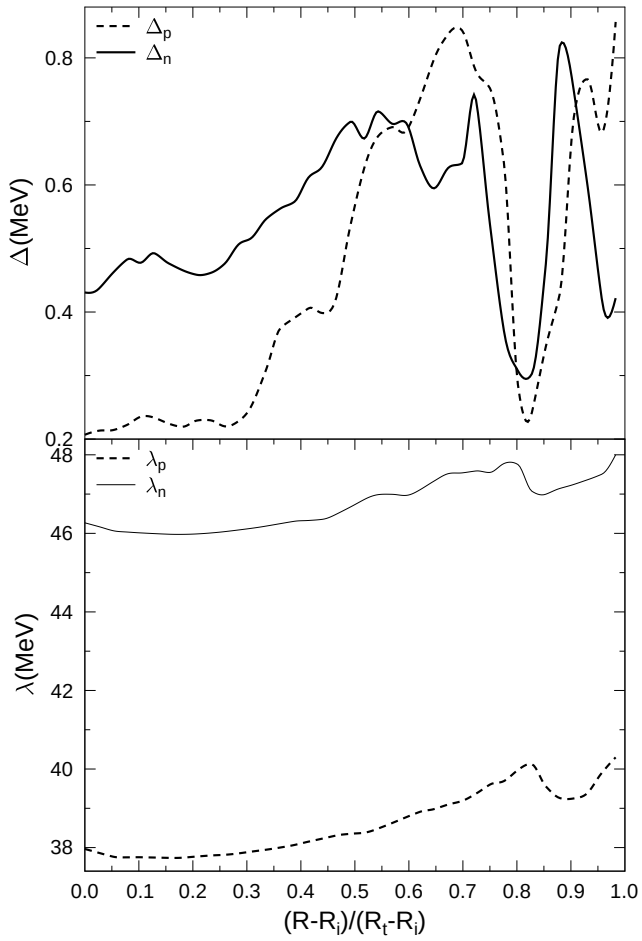


FIG. 7. (Color online) Solutions of BCS equations for symmetrical fission of ^{282}Cn with inearly increasing R_2: the gap for protons and neutrons (top) and the Fermi energy for protons and neutrons (bottom).

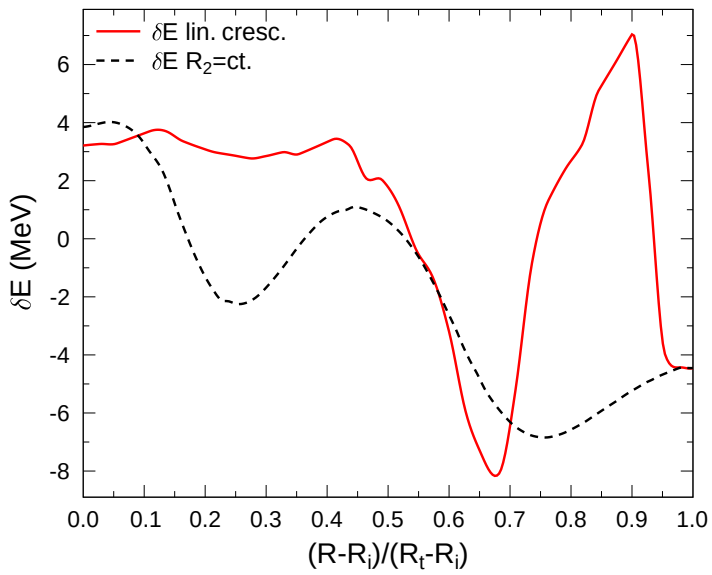


FIG. 8. (Color online) Comparison of shell plus pairing effects for fission of ^{240}Pu with linearly increasing R_2 and constant R_2.

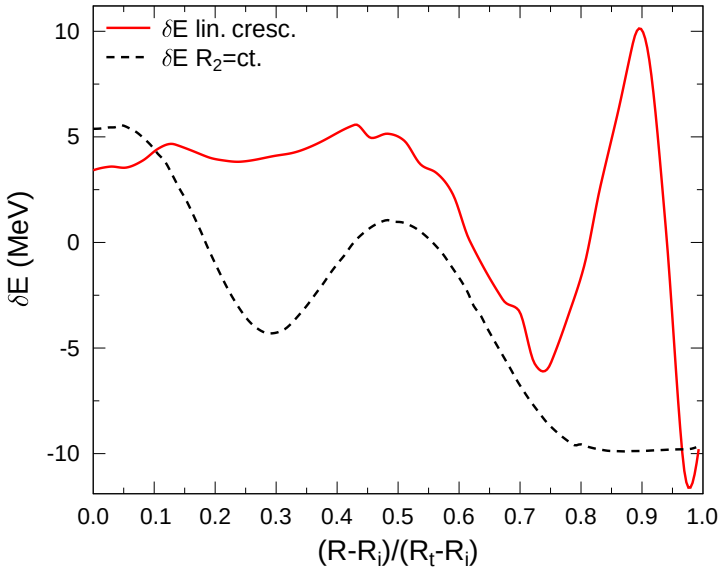


FIG. 9. (Color online) Comparison of shell plus pairing effects for fission of ^{252}Cf with linearly increasing R_2 and constant R_2.

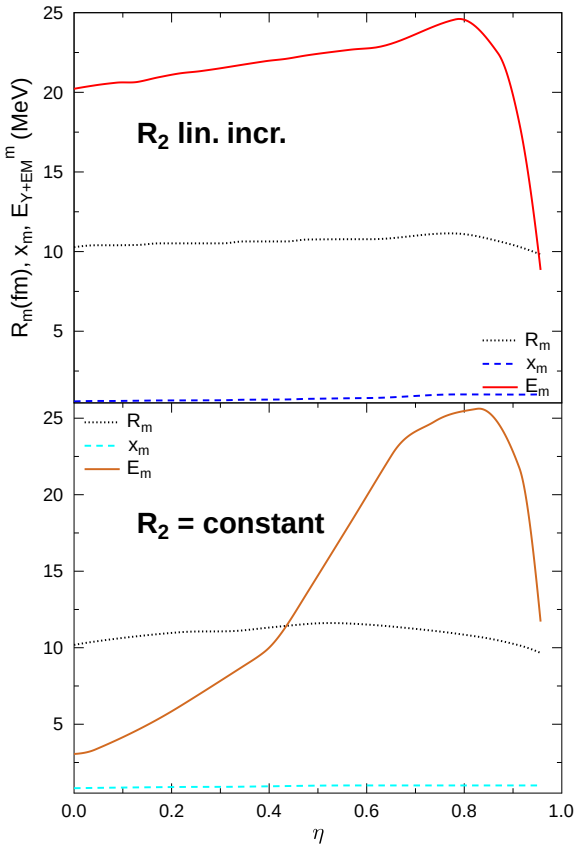


FIG. 10. (Color online) Position and value of maximum Y+EM model deformation energy versus mass asymmetry, η, for fission of ^{282}Cn with linearly increasing R_2 (top) and constant R_2 (bottom).

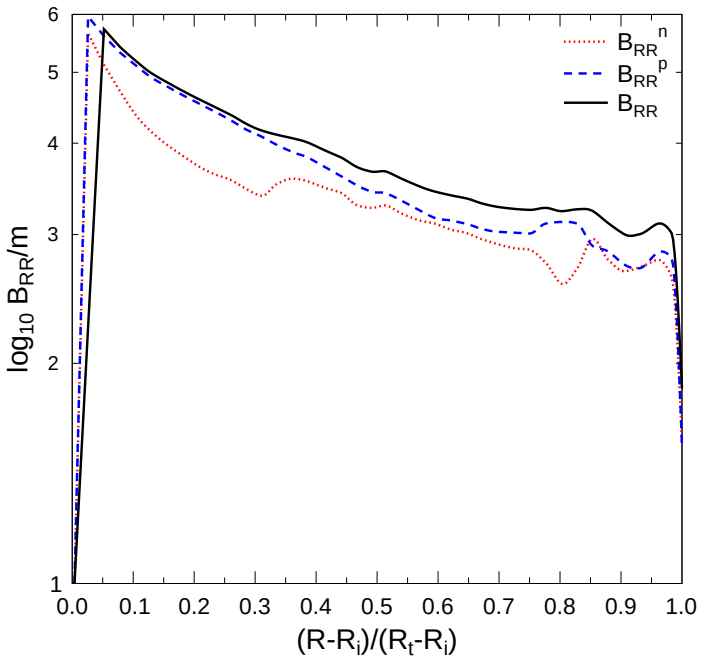


FIG. 11. (Color online) Decimal logarithm of the dimensionles RR component of nuclear inertia tensor for symmetrical fission of ^{282}Cn with linearly increasing R_2.

TABLE I. Statics. Minima and maxima of deformation energy in MeV for fission of ^{282}Cn. Linearly increasing R_2. x_{exit} corresponds to $E_v = 0$.

η	x	1st min.	x	1st max.	x	2nd min.	x	2nd max.	x_{exit}
0.000	0.000	0.000	0.580	29.114	0.820	7.340	0.900	14.720	1.15
0.043	0.000	0.000	0.580	29.371	0.840	7.211	0.900	14.550	1.15
0.087	0.000	0.000	0.600	29.515	0.840	7.573	0.920	15.045	1.25
0.130	0.000	0.000	0.600	29.817	0.860	7.447	0.940	14.884	1.27
0.174	0.000	0.000	0.620	29.911	0.880	7.525	0.960	15.033	1.34
0.217	0.000	0.000	0.620	30.172	0.900	7.452	0.980	15.853	1.40
0.261	0.000	0.000	0.640	30.267	0.900	7.751	1.000	15.488	1.44
0.304	0.000	0.000	0.640	30.090	0.920	7.211	0.980	17.500	1.45
0.348	0.000	0.000	0.640	30.327	0.940	8.563	1.040	15.755	1.46
0.391	0.000	0.000	0.680	30.585	0.960	8.616	0.980	10.345	1.34
0.435	0.000	0.000	0.700	30.647	1.000	5.873	1.000	5.873	1.33
0.478	0.000	0.000	0.720	30.938					1.46
0.522	0.000	0.000	0.760	29.417					1.68
0.565	0.000	0.000	0.860	31.420					1.73
0.609	0.000	0.000	0.880	31.611					1.85
0.652	0.000	0.000	1.180	31.258					2.06
0.696	0.000	0.000	1.200	34.233					2.39
0.739	0.000	0.000	1.220	33.409					2.40
0.783	0.000	0.000	1.240	35.149					2.80
0.826	0.000	0.000	0.960	40.492					3.18
0.870	0.000	0.000	0.960	36.532					4.23
0.913	0.000	0.000	0.940	35.736					7.11
0.956	0.000	0.000	0.940	18.891					13.99

TABLE II. Statics. Minima and maxima of deformation energy in MeV for fission of ^{282}Cn. Constant R_2. x_{exit} corresponds to $E_v = 0$.

η	x	1st min.	x	1st max.	x	2nd min.	x	2nd max.	x_{exit}
0.000	0.100	-1.458	0.260	0.737	0.420	-1.480	0.700	3.596	0.950
0.043	0.100	-1.323	0.260	1.390	0.440	-1.910	0.720	3.151	0.950
0.087	0.100	-1.114	0.280	2.102	0.460	-2.061	0.740	3.950	1.045
0.130	0.100	-0.920	0.300	2.845	0.500	-1.779	0.840	5.966	1.110
0.174	0.100	-0.715	0.300	3.639	0.520	-1.061	0.920	8.926	1.135
0.217	0.100	-0.529	0.340	4.467	0.540	0.029	0.940	11.298	1.165
0.261	0.100	-0.346	0.360	5.334	0.580	1.227	0.960	12.084	1.175
0.304	0.100	-0.226	0.400	5.796	0.600	2.502	0.980	13.256	1.190
0.348	0.060	-0.117	0.420	6.534	0.660	2.737	0.980	9.722	1.170
0.391	0.060	-0.031	0.440	7.148	0.740	2.226	1.000	4.888	1.150
0.435	0.000	0.000	0.480	7.920	0.820	2.640	1.040	4.173	1.150
0.478	0.000	0.000	0.540	9.079	0.840	6.493	1.060	8.094	1.190
0.522	0.000	0.000	1.060	14.358					1.670
0.565	0.000	0.000	1.080	19.183					1.696
0.609	0.000	0.000	1.080	24.061					1.644
0.652	0.000	0.000	1.100	27.366					2.107
0.696	0.000	0.000	1.100	30.978					2.051
0.739	0.000	0.000	1.120	31.256					2.447
0.783	0.000	0.000	1.140	32.228					2.461
0.826	0.000	0.000	1.180	33.117					3.454
0.870	0.040	-0.032	1.220	31.574					3.952
0.913	0.080	-0.093	1.280	25.607					6.933
0.956	0.200	-0.394	1.808	13.786					8.266